DOUGLAS PAPER NO. 1774

DYNAMIC ENVIRONMENTS OF THE S-IV AND S-IVB SATURN VEHICLES

BY
R.W. MUSTAIN
ACOUSTICS AND STRUCTURAL DYNAMICS SECTION
DOUGLAS AIRCRAFT COMPANY, INC.
MISSILE & SPACE SYSTEMS DIVISION
SPACE SYSTEMS CENTER
5301 BOLSA AVENUE
HUNTINGTON BEACH, CALIFORNIA

PRESENTED TO
THE 33RD SYMPOSIUM ON SHOCK, VIBRATION AND ASSOCIATED ENVIRONMENTS, OFFICE OF THE SECRETARY OF DEFENSE, WASHINGTON, D.C.
DECEMBER 5, 1963

DOUGLAS MISSILE & SPACE SYSTEMS DIVISION

ABSTRACT

The vibration and acoustic environments of the S-IV and S-IVB Stages of the Saturn vehicle are summarized. A brief review of techniques used to predict the dynamic environments of the S-IV and S-IVB vehicles is presented. This review includes discussions on the prediction of rocket exhaust noise, boundary layer noise, sinusoidal vibrations, and random vibrations for the S-IV and S-IVB vehicles. In addition, sine-random vibration conversions are given.

Various prediction techniques are examined and compared. Predictions of S-IV and S-IVB rocket exhaust noise are compared with field measurements. Different methods of acoustic/vibration correlativity are utilized to provide environmental vibration levels for the S-IV and S-IVB vehicles. A curve of classical vibration response to acoustic loading is given for use in the correlation of acoustic levels with structural vibration levels. The prediction of both sinusoidal and random vibrations is presented in considerable detail to provide illustrative examples. Typical tables of computations are included.

INTRODUCTION

A primary design consideration for the Saturn S-IV and S-IVB Stages is the effect of acoustical and vibrational excitations on the vehicle structure and on delicate airborne equipment. The importance of this consideration is enhanced by noting the severe dynamic environments which are produced by the high-thrust rocket systems of the Saturn Vehicle. In addition, attention must be given to the possible damaging effects of aerodynamic noise which results from turbulence in the boundary layer; this noise approaches its highest level during the maximum Q (dynamic pressure) phase of the flight mission. In view of the high-thrust rocket systems and the boundary layer noise excitations, there exists a fundamental requirement for an adequate definition of the dynamic environments of the S-IV and S-IVB Stages of the Saturn Vehicle. The definition of these environments is continually being up-dated; therefore, this paper presents only an interim report. The definition of the S-IV and S-IVB dynamic environments is being modified and improved progressively by field measurements and more refined prediction studies.

The acoustic and vibrational environments of the S-IV and S-IVB Stages of the Saturn Vehicle are discussed in this paper. Predictions and measurements of these dynamic environments are presented. Predicted acoustic time histories are given for the early phases of the S-IV and S-IVB missions. These time histories are compared with acoustic measurements from two flights of the Saturn I Vehicle. Prediction techniques for rocket exhaust noise and boundary layer noise are discussed briefly. Predictions of acoustic spectra for six S-IV engines (RL-10), without diffuser attenuation, are given. Measurements of acoustic levels during firings of the S-IVB engine are presented and compared with predicted levels.

Different methods of acoustic/vibration correlativity are utilized to provide environmental vibration levels for both the S-IV and S-IVB Stages. Various correlation techniques are compared and evaluated. A curve of classical vibration response to acoustic loading is given for use in the correlation of acoustic levels with structural vibration levels. Acoustic/vibration correlation methods are used to determine both sine and random vibration environments. Also, sine-random vibration conversions are used to establish random vibration levels for the S-IVB Stage.

SATURN CONFIGURATIONS

The S-IV, powered by six RL-10 engines, is the second stage of the Saturn I; and the S-IVB, powered by one J-2 engine, is (1) the second stage of the Saturn IB and (2) the third stage of the Saturn V (See Figure 1). The primary mission of the Saturn I configuration is unmanned orbital flights around the earth. The Saturn IB configuration has as its primary mission the support of the basic Apollo mission by early testing of Apollo spacecraft modules in earth orbital enviroments. The Saturn V is a three-stage vehicle whose primary mission is lunar manned operations.

THE ACOUSTIC ENVIRONMENTS

The structure and the equipment on the S-IV and S-IVB Stages will be exposed to acoustic forcing functions that are variant with time and the mission profile. The following list of forcing functions presents some of the acoustic sources that must be considered during the Saturn program (reference 1):

1. rocket engine noise
2. ancillary equipment
3. laminar boundary layer noise
4. turbulent boundary layer fluctuations
5. turbulent wakes (protuberated)
6. base pressure fluctuations
7. cavity resonances
8. secondary acoustic sources

Usually, the sound field of the rocket engine is the most important source of vibration, and the boundary layer noise ranks second in source severity; however, preliminary data show that the boundary layer noise on the S-IV and S-IVB Stages is equal to or greater than the rocket engine noise at some locations. This condition is being investigated; additional measurements will be made during Saturn flights. During the launch phase of the Saturn Vehicle, the tremendous noise generated by the rocket engines is transmitted through the atmosphere and reflected by the ground plane around the space vehicle. Since the rocket noise is essentially random and "white" in nature, it creates resonant responses of skin panels and structures. The magnitude of this excitation depends upon the frequency spectrum, the amplitude, the space correlation of the noise, and the mechanical impedance of the structure. The resulting vibrational energy is transferred

throughout the vehicle to substructure and equipment. Some of the panels act as secondary noise sources and radiate acoustic energy into the vehicle's compartments. In turn, some of these bays become semi-reverberant chambers to maintain fairly high acoustic levels. Rocket engine noise, reflected from the ground plane, dominates the Saturn environment for the first few seconds of flight until the Saturn Vehicle rises a distance equivalent to approximetely 50 exit nozzle diameters. After the Saturn Vehicle leaves the launch pad, it begins to gain velocity; and then the effect of vehicle motion becomes apparent until, on approaching Mach one, the rocket noise does not propagate to the vehicle. As the Saturn Vehicle moves with increased velocity through the atmosphere, boundary layer noise becomes the dominant forcing function. Originally, the boundary layer noise is extremely low and is masked during the launch phase by the intense rocket engine noise, and is not propagated in any degree until the sonic speed range is reached. The boundary layer noise is a function of dynamic pressure and other related aerodynamic parameters such as the vehicles attitude, and configuration; this noise reaches its highest level during the maximum Q phase of the flight mission.

Figure 2 summarizes the acoustic environment of the S-IV and S-IVB Stages during the first 160 seconds of the flight mission. This chronological history of the major acoustic sources depicts (1) the sound pressure levels predicted for the S-IV and S-IVB Stages and (2) the sound pressure levels measured during Saturn I flights SA-3 and SA-4. The launch phase, the diminution immediately after launch, the increase in level to the maximum dynamic pressure, and the final decline to negligible noise levels are included in this summation. This set of curves shows that the boundary layer noise is equal to or greater than the rocket engine noise during the flight mission. These boundary layer noise levels are indicative of local flow conditions with large protuberances, and may be much less (approximately 14 db) on cleaner areas of the S-IV and S-IVB Stages where undisturbed boundary layer flow occurs. Four individual time history curves are displayed in Figure 2:

1. the predicted S-IV acoustic time history
2. the predicted S-IVB acoustic time history
3. acoustic measurements obtained during the Saturn SA-3 flight internally on the SI Stage
4. acoustic measurements obtained during the Saturn SA-4 flight externally on the S-IV aft interstage

M-14461

SATURN CONFIGURATIONS

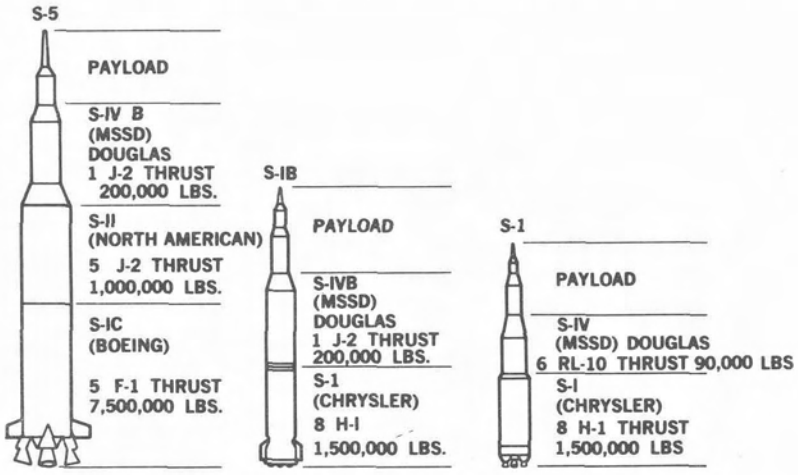

FIGURE 1

M-14465

S-IV AND S-IVB ACOUSTIC TIME HISTORIES

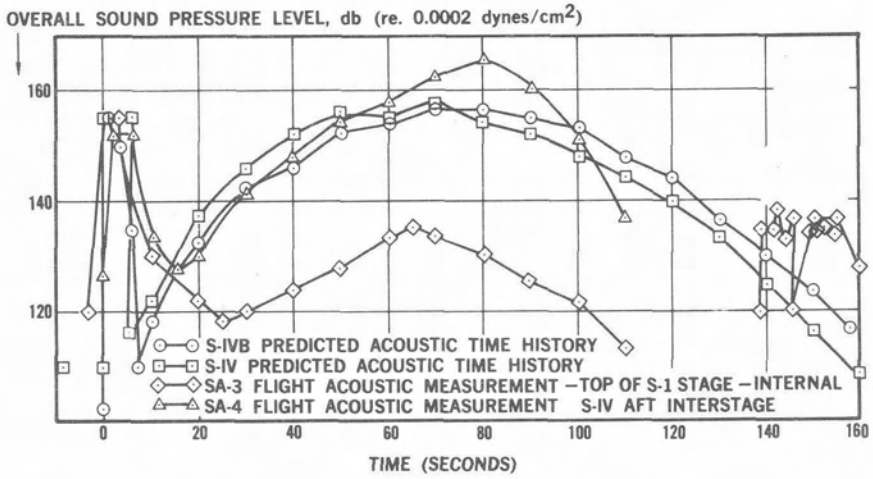

FIGURE 2

All of these curves show a reasonable likeness during the launch phase. With the logical exception of the SA-3 data, the curves also show good agreement during the maximum Q phase of the mission. That is, the SA-3 microphone was located on the lower SI Stage, was an internal measurement, and consequently, the SA-3 data should not correlate well with the other data during the maximum Q phase. Since the microphone on the SI Stage is the closest acoustic measurement to the S-IV Stage, the SA-3 data are presented only for general interest. The microphone on the fourth Saturn flight (SA-4) was mounted flush with the skin of the S-IV aft interstage in a disturbed flow region. Incidentally, the S-IV Stages on the SA-3 and SA-4 flights were dummy stages. The highest boundary layer noise levels on Figure 2 are those measured during the SA-4 flight. As a first approximation, these fluctuations are assumed proportional to the freestream pressure:

$$\text{OAFPL or OASPL} \cong 20 \log Q + K \quad \text{db} \qquad (1)$$

where OAFPL is the level of the overall pressure fluctuations at the surface, Q is the freestream dynamic pressure in lbs/sq.ft., and K is a factor which varies with aerodynamic flow parameters. K is a function of the vehicle's altitude, attitude, velocity, and configuration. The value of K will be approximately 86 for an aerodynamically clean configuration with a zero angle of attack. As drag increases, the value of K increases. Recent wind tunnel tests performed at Douglas indicate that space vehicles, such as the Saturn, with large protuberances, have related K factors as great as 110. A K value of 100 was used to determine the S-IV and S-IVB predictions on Figure 2. The protuberances are external vehicle items such as wiring ducts, fuel ducts, ullage rockets, and the like.

Predictions of rocket engine noise from six RL-10 engines, without diffusers, are shown in the three-dimensional display of Figure 3. The sound pressure levels are given as a function of octave bands and location forward of the engine nozzles. These levels are extremely conservative since the S-IV Stage is static (or acceptance) fired with 27 foot diffusers which exhaust against a deflector plate; therefore, these levels should be lowered considerably for S-IV static firings. Two different prediction methods, described in Reference 2, were used to calculate the noise from the RL-10 engine. The 15,000 pound thrust engine produces a sound power level of approximately 181 db overall (re 10^{-13} watts). The value of 181 db was found by using an empirical equation which was based on data from rockets in the 1,000 to 130,000 pounds thrust range (Reference 3):

$$OAPWL = 78 + 13.5 \log_{10} W_m \qquad (2)$$

where W_m = mechanical power of jetstream in watts,

$W_m = 0.676\ tV = 0.676\ (t^2 g)/w$,

with $V = (tg)/w$ = gas velocity at nozzle exit in fps,

t = thrust in pounds,

g = acceleration due to gravity = 32.2 ft/sec^2,

w = weight flow in lb/sec

then $PWL = 78 + 13.5 \log 0.676 \frac{t^2 g}{w}$

The empirical relationship of equation (2) remains a fairly reliable prediction of the total acoustical power of conventionally fueled rockets at sea-level operations (Reference 4).

Acoustic data obtained during test stand firings of the S-IVB engine, the J-2, at Rocketdyne are summarized in Figure 4. The average sound pressure levels from four test firings are plotted as a function of octave bands and distance forward of the nozzle exit plane. Acoustic data, from Figure 4, for the aft skirt are replotted in Figure 5 and compared with acoustic levels which were determined by four different prediction methods:

1. WADC TR 58-343 (Reference 5)
2. WADC TR 57-354 (Reference 3)
3. Modified WADC TR 58-343 (Reference 6)
4. Scaled Thor data

The highest levels on Figure 5 are displayed by the measured J-2 data, especially in the second through fifth octave bands. The scaled Thor data and the modified WADC data show a reasonable agreement with the measured data at the higher frequencies. Following are the original measured data on the Thor booster:

Octave Band	Sound Pressure Level
	db
1	141
2	144
3	146
4	147
5	146
6	145
7	144
8	143
overall	154

M-14469

PREDICTED ACOUSTIC SPECTRA
6 RL-10 ENGINES WITHOUT DIFFUSER ATTENUATION

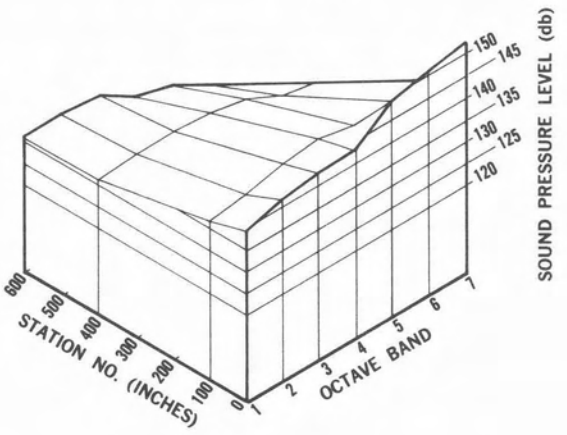

FIGURE 3

M-14468

MEASURED S-IVB ENGINE ACOUSTIC SPECTRA

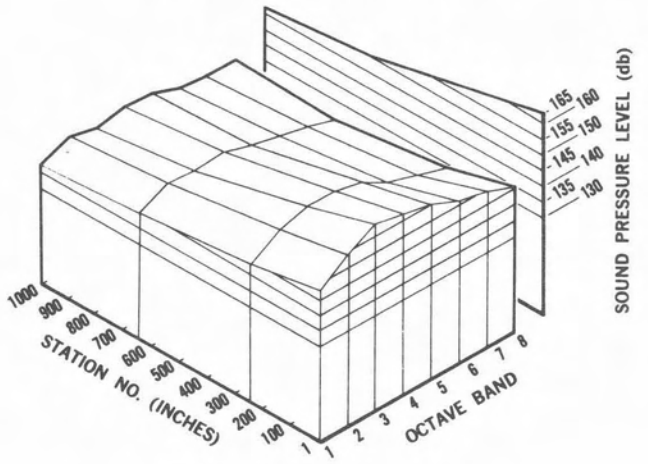

FIGURE 4

Using equation (2), the sound power levels were found to be 199 db re 10^{-13} watt for the Thor and 198 db re 10^{-13} watt for the J-2 engine at sea level. Then, the sound power level differential of one db was subtracted from the original Thor data. These lower levels are plotted on Figure 5 as the scaled Thor data.

S-IV VIBRATION PREDICTIONS AND MEASUREMENTS

Saturn rocket engine and boundary layer noise has, in general, a random distribution with broad spectra. As these acoustic excitations impinge on the S-IV Stage they induce random vibrations (with variant bandwidths) on the vehicle structure. This condition of randomness varies throughout the vehicle as the spectra are influenced by structural filters that create dominant peaks at response frequencies. Also, the random vibrations are assumed to have instantaneous accelerations (in any frequency band) that exhibit normal or Gaussian distributions. Perhaps, the most severe vibration environment occurs during the maximum Q phase of flight for a relatively short period of time. Lower vibration levels occur on the S-IV Stage during the acceptance (static) firings which are conducted on each S-IV Stage at the Sacramento, California facility of the Douglas Aircraft Company, Inc. The vibration levels during the S-IV acceptance firings are greatly reduced by the use of 27 foot diffusers which attenuate the acoustic excitations from the RL-10 engines. In addition, the S-IV Stage is supported by isolators during the acceptance firings to minimize the dynamic feedback from the test stand. Hence, the vibration environment of the S-IV Stage during the acceptance firings is primarily mechanically induced. Furthermore, it is highly probable that the vibration environment of the acceptance firings closely simulates the vibration environment during flight when the RL-10 engines are firing. In order to establish the vibration environment of the S-IV acceptance firings, vibration measurements were recorded during static firings of the S-IV-5 Stage at Sacramento. Some of these data are presented in this report and compared with vibration predictions based on the conservative acoustic levels of Figure 3.

Prior to discussing these vibration comparisons, a brief description is given of acoustic/vibration correlation techniques which are used in this paper to predict some of the S-IV vibration levels. Several investigators have attempted to establish the relationship between the acoustic forcing function and the resultant vibratory response. This has led to the establishment of vibration prediction techniques which are founded on acoustic/

S-IVB STATIC FIRING ACOUSTIC SPECTRA AT AFT SKIRT

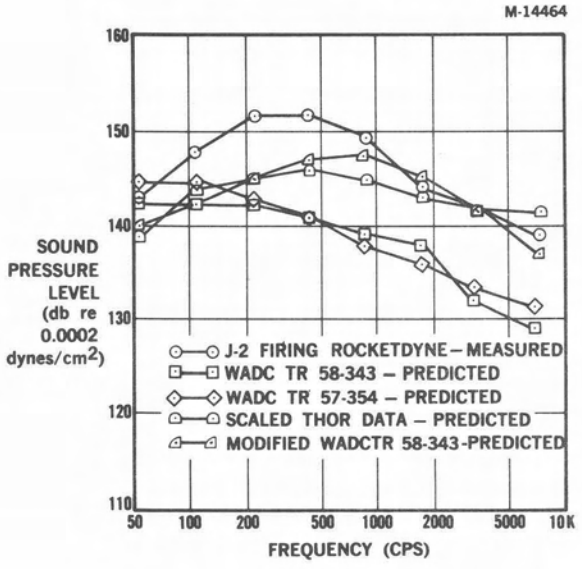

FIGURE 5

vibration correlativity. These prediction methods have used empirical information as their basis. Much remains to be desired on the accuracy of these various methods. The fault lies in the fact that these prediction methods are based on general data; consequently, these methods may not provide optimum predictions for specific cases.

Another drawback of most prediction techniques is the failure to account for structural resonances caused by structural filters. To explain further, predictions of random vibrations should display dominant peaks at response frequencies. However, most predictions show broad spectra which are in general agreement with typical vibration test specifications. This leads to conservative vibration test levels which may or may not be justified: This depends on the structural configuration. Relatively soft structures with many response frequencies should be tested to conservative specifications with broad spectra. In contrast, strong primary structure with a high natural frequency will have a dominant response peak. Then, the environmental vibrations on such a structure are best represented or estimated by a peaked vibration spectrum. Thus, ideal predictions should be based on actual knowledge of the structure being investigated. First, analytical techniques can be used to determine response spectra of structures. Secondly, response frequencies of structures can be determined by actual measurements. Finally, it can be expected that, within this decade, mechanical admittance or impedance measurements will be widely used to define structural response spectra and to determine transfer functions.

One of the popular empirical methods used to predict vibration levels is described in Reference 7. Reference 7 provides curves for predicting vibrations induced by acoustic excitations. Predictions using Reference 7 data can be determined for different confidence levels. However, these resulting vibration spectra are broad band such as those found in typical test specifications. Two additional curves for predicting acoustically induced vibrations are given in Figures 6 and 7. The correlation data of Figure 6 are based on Minuteman, Jupiter, Titan, and Skybolt measurements collected by E. F. Winter (Reference 8). The acoustic/vibration correlativity of Figure 7 was compiled by the author of this paper. The data in Figure 7 are representative of rigid primary structure with a dominant and high (say approximately 700 to 1200 cps) response frequency. These data tend to follow a classical transmissibility curve.

M-14473

STRUCTURAL RESPONSE TO ACOUSTIC LOADING

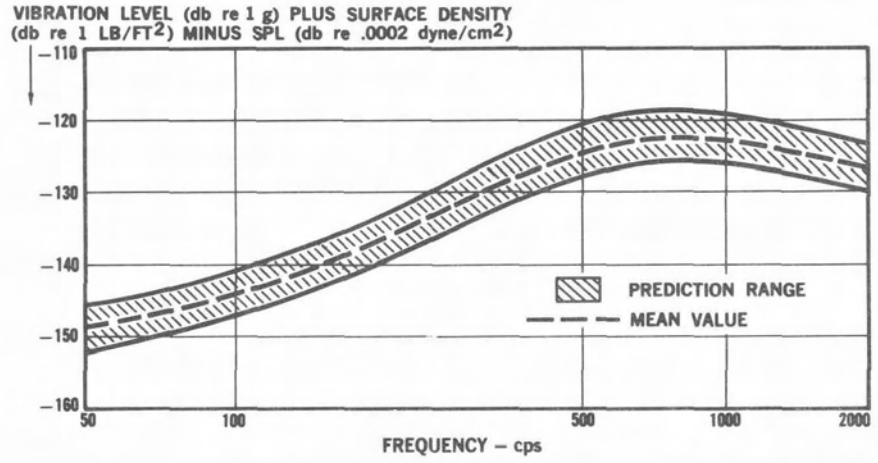

FIGURE 6

M-14474

CLASSICAL RESPONSE TO ACOUSTIC LOADING

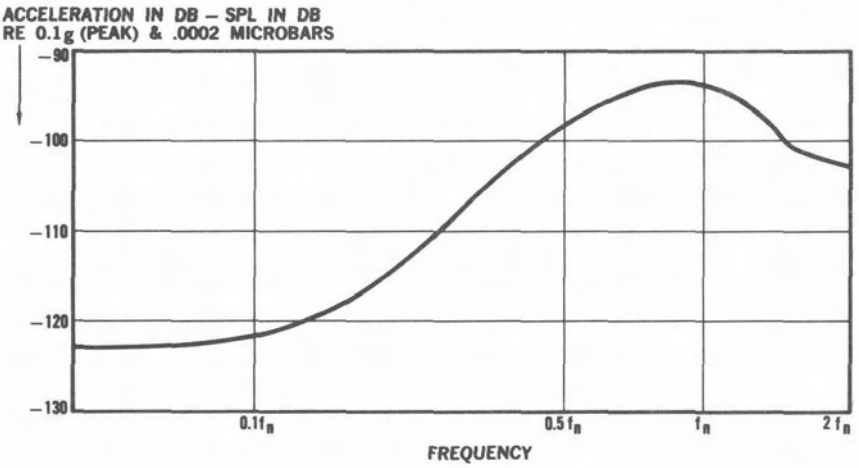

FIGURE 7

A large quantity of useful vibration data was obtained during two acceptance firings of the S-IV-5 Stage. The presentation of all the vibration data from the S-IV-5 firings is beyond the scope of this paper. The accelerometer locations during the S-IV-5 acceptance firings at Sacramento are shown in the sketch of Figure 8. Data from only three accelerometer locations are given in this report. Acceptance firing vibrations at the gimbal point, the thrust cone, and the base of the telemetry rack are displayed in Figures 9, 10, and 11. In these three figures, the acceptance firing vibrations are compared with predictions of acoustically induced vibrations which are based on the RL-10 engine data of Figure 3. These predictions were established by using data from Figures 3, 6, and 7 of this paper and data from Reference 7. Four curves are shown in each of the graphs of figures 9, 10, and 11:

1. vibration levels determined by the method of reference 7 (95% confidence, Smith and Mahaffey)
2. vibration levels determined by using the data in Figure 6 of this paper
3. vibration levels determined by using the data on the classical curve of Figure 7
4. measured vibration levels from the acceptance firings of the S-IV-5 Stage at Sacramento, California

Three tables showing typical data for each of the prediction methods are given in addendum A which accompanies this paper.

The predicted vibration levels in Figures 9, 10, and 11 are based on the acoustic levels shown in Figure 3; consequently, these predicted vibrations are much greater than the actual acoustically induced vibrations on the S-IV acceptance firings. Since the actual S-IV acceptance firings are made with diffusers, the static firing acoustic levels are much lower than the levels of Figure 3. In turn, the acoustically induced vibrations during the static firings are much less than the predictions in Figures 9, 10, and 11. Whereas the S-IV acceptance firings are made with diffusers which attentuate most of the sound, the vibrations on the S-IV Stage during the acceptance firings are almost entirely mechanically induced. A study of Figures 9, 10, and 11 shows that the mechanically induced vibrations during the acceptance firings are approximately equal to predicted acoustically induced vibrations from six unattenuated RL-10 engines. Originally, these figures were prepared to show the differential between mechanically induced

M-14457

ACCELEROMETER LOCATIONS ACCEPTANCE FIRING S-IV-5

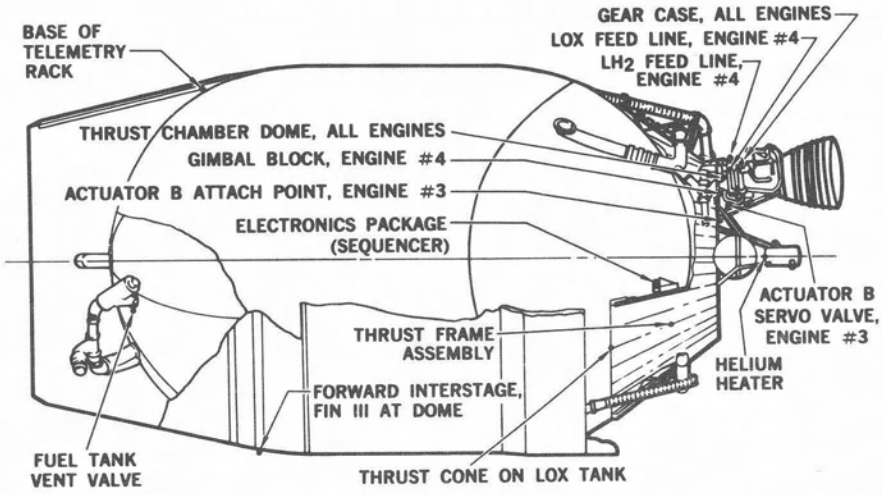

FIGURE 8

M-14467

COMPARISON OF S-IV-5 ACCEPTANCE FIRING VIBRATIONS WITH PREDICTED VIBRATIONS BASED ON DATA FROM FIGURE 3

GIMBAL POINT

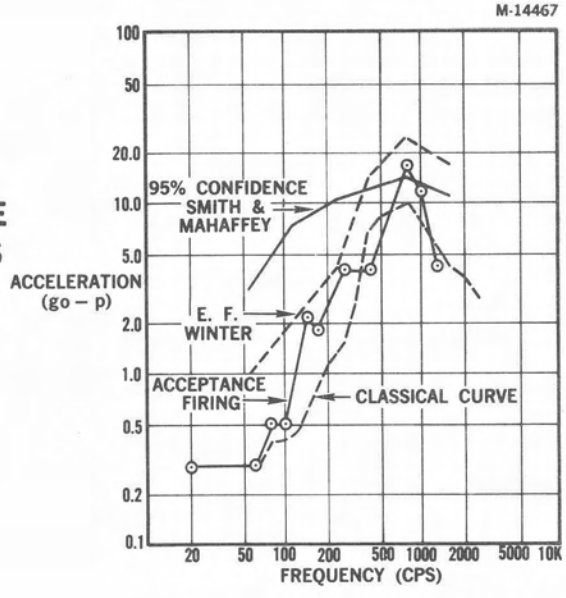

FIGURE 9

COMPARISON OF S-IV-5 ACCEPTANCE FIRING VIBRATIONS WITH PREDICTED VIBRATIONS BASED ON DATA FROM FIGURE 3

THRUST CONE

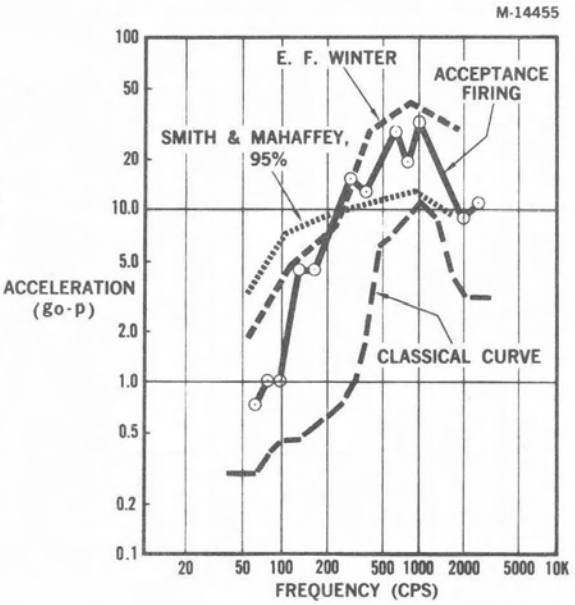

FIGURE 10

COMPARISON OF S-IV-5 ACCEPTANCE FIRING VIBRATIONS WITH PREDICTED VIBRATIONS BASED ON DATA FROM FIGURE 3

BASE OF T/M

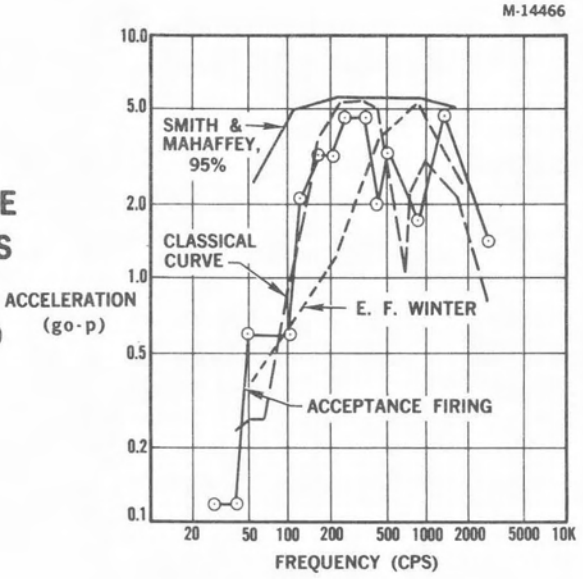

FIGURE 11

vibrations (acceptance firing data) and acoustically induced vibrations (the predicted vibrations). However, the predicted and the measured vibrations show an unexpected agreement which indicates that the S-IV engine/vehicle transfer function results in relatively high mechanically induced vibrations. This transfer function includes the effects of multiple engine dynamics on the S-IV structure. Also, some of the mechanically induced vibrations may be attributed to accessories on the six RL-10 engines. This subject of mechanically and acoustically induced vibration on the S-IV Stage is an interesting one that requires further analysis. This relationship will be better defined as microphone measurements and additional vibration measurements become available from future S-IV acceptance firings.

The next four figures, 12 through 15, show predictions of the acoustically induced vibrations during launch and flight of the S-IV Stage (Reference 9). In each figure, an envelope has been drawn over the 95% confidence level (Smith and Mahaffey) to provide a conservative test level. This test level is applied as a one minute per octave sinusoidal logarithmic sweep. With this sweep rate, a test specimen is exposed to each resonance for approximately 35 seconds (Reference 9). Predicted vibrations on the extreme aft S-IV interstage are plotted on Figure 12. The vibration environment of Figure 12 is based on wind tunnel data for the maximum Q phase and on SI acoustic data for the lift-off phase. Both the maximum Q and the lift-off predictions of Figure 12 were determined by using the data from Reference 7. The vibration environments of the aft interstage (Figure 13), the thrust structure (Figure 14), and the forward interstage (Figure 15) are based on acoustic data which were obtained from the Saturn SA-4 flight and from SI Stage static firings. Figures 13, 14, and 15 display comparative vibration levels which were obtained by using the data of Figures 6 and 7 of this paper and the data from Reference 7. Curves A, C, and D display a reasonable agreement. The best agreement is noted near the response frequence of the structure where curves C and D peak. The poorest correlation can be found at the lower frequencies where the broad spectrum of curve A exists. Curve A is typical of specifications which provide overly conservative test levels. The reason for the difference in the low frequency levels is probably due to the fact that curve A is an envelope of vibration levels of light components attached to light flexible structure. Curves B, C, and D are considered to envelope vibration levels measured on heavy primary structure.

M-14456

PREDICTION OF ACOUSTICALLY AND PRESSURE FLUCTUATION INDUCED VIBRATION-EXTREME AFT OF S-I/S-IV INTERSTAGE

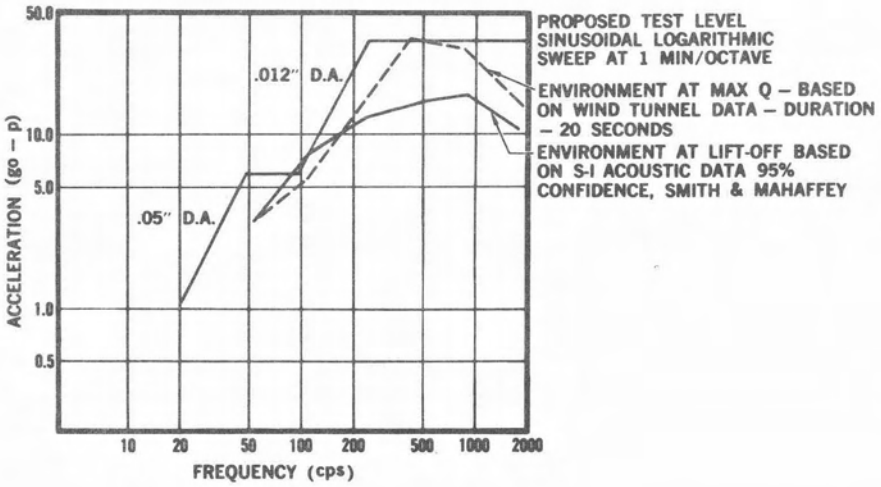

FIGURE 12

M-14460

PREDICTIONS OF ACOUSTICALLY INDUCED VIBRATION-AFT INTERSTAGE OF S-IV

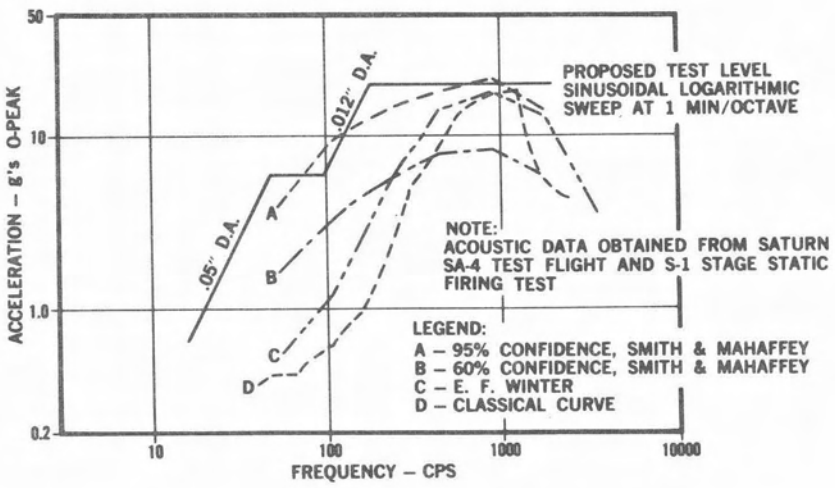

FIGURE 13

M-14459

PREDICTIONS OF ACOUSTICALLY INDUCED VIBRATION-THRUST STRUCTURE OF S-IV

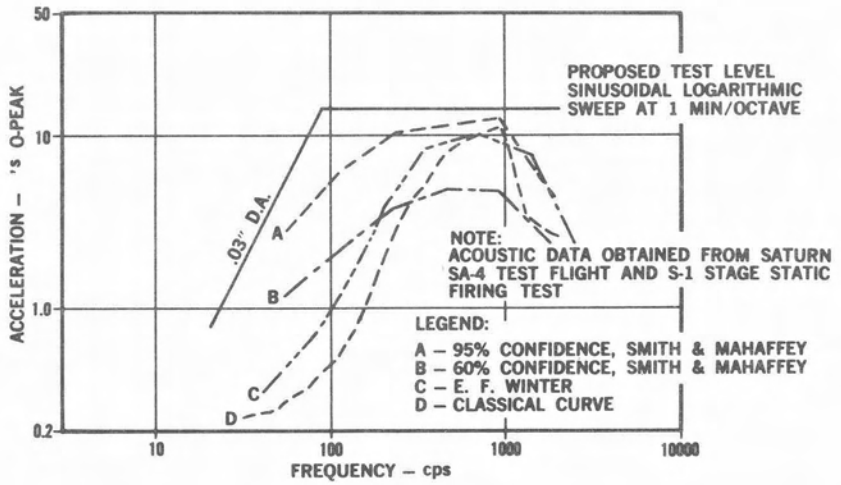

FIGURE 14

M-14458

PREDICTIONS OF ACOUSTICALLY INDUCED VIBRATION-FORWARD INTERSTAGE OF S-IV

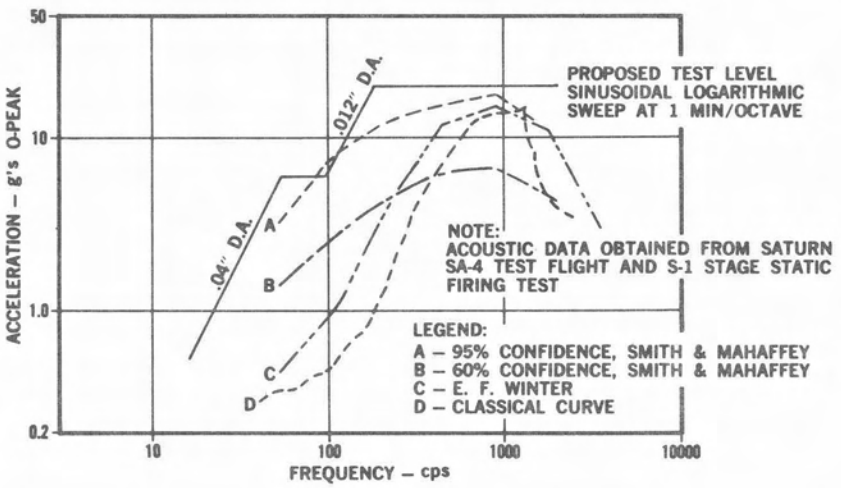

FIGURE 15

S-IVB VIBRATION PREDICTIONS

An exploded view of the Saturn S-IVB Stage is presented in Figure 16. Similar to the S-IV dynamic environment, the S-IVB vibration environment has, in general, a random distribution with broad spectra. The bandwidth of these random vibrations varies throughout the vehicle as the spectra are influenced by structural filters that create dominant peaks at response frequencies. Furthermore, the instantaneous accelerations are assumed to have normal distributions or slight modifications of the normal distribution, and the corresponding peaks are assumed to be distributed according to the Rayleigh law. The S-IVB vibrations will be significant during the lift-off phase, the maximum Q phase, and the J-2 engine firing phase. The lift-off vibrations and the maximum Q vibrations of the S-IVB Stage will be similar in severity to the S-IV lift-off and maximum Q vibrations. The vibrations during the S-IVB acceptance firings will be greater than the vibrations during the S-IV acceptance firings because of the more severe acoustical environment. Likewise, the mechanically induced vibrations from the J-2 engine during S-IVB flight will be greater than the flight vibrations from the RL-10 engines on the S-IV Stage because of the increased engine size and thrust. Since the vibrations during the S-IVB acceptance firings will rank high in importance, predictions have been made of acoustically induced vibrations on the S-IVB static firings.

These predictions were established by using data from Figures 4, 6, 7, and 17 of this paper and data from Reference 7. Figure 17 of this paper was originally presented in Reference 10. This figure is useful in proposal stages and early design stages where little is known about a vehicle. To use this figure, only an overall sound pressure level is required; this technique provides a reasonable "ball-park" estimation. Random vibration spectra are given for five different overall sound pressure levels in Figure 17. Only random vibration predictions are given for the S-IVB acceptance firings. Predicted random vibration levels for the S-IVB acceptance firings are given in Figures 18 and 19. Five curves are shown in each of the graphs of Figures 18 and 19:

1. vibration levels determined by the methods of Reference 7 (95% confidence, Smith and Mahaffey)
2. vibration levels determined by the method of Reference 7 (60% confidence, Smith and Mahaffey)
3. vibration levels determined by using the data in Figure 6 of this paper

M-14463

SATURN S-IVB STAGE EXPLODED VIEW

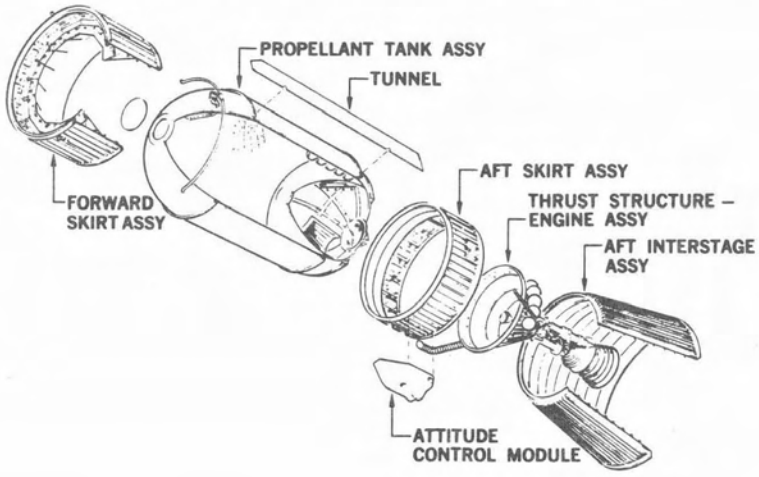

FIGURE 16

M-14462

TEST REQUIREMENT ENVELOPES FOR VARIOUS ACOUSTIC NOISE LEVELS

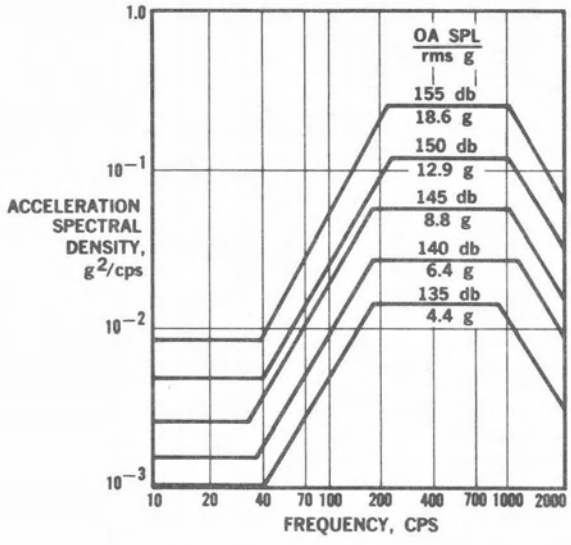

FIGURE 17

M-14470

PREDICTED RANDOM VIBRATION LEVELS
S-IVB AFT SKIRT STATIC FIRING

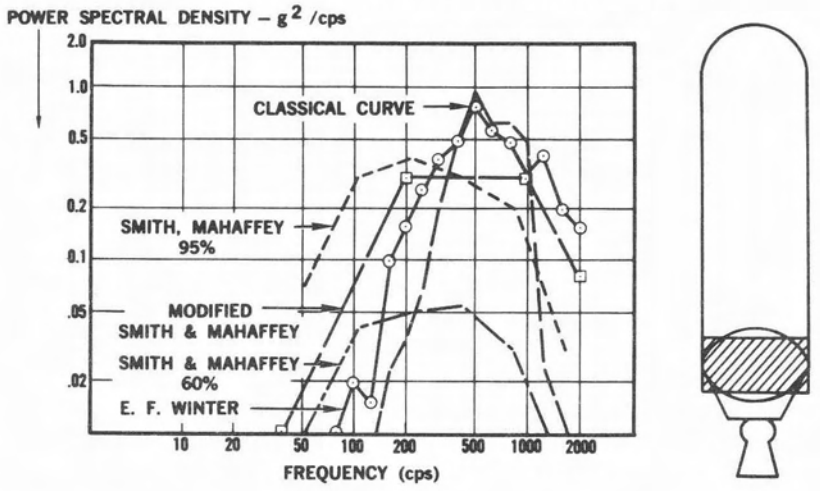

FIGURE 18

M-14472

PREDICTED RANDOM VIBRATION LEVELS
S-IVB FORWARD SKIRT STATIC FIRING

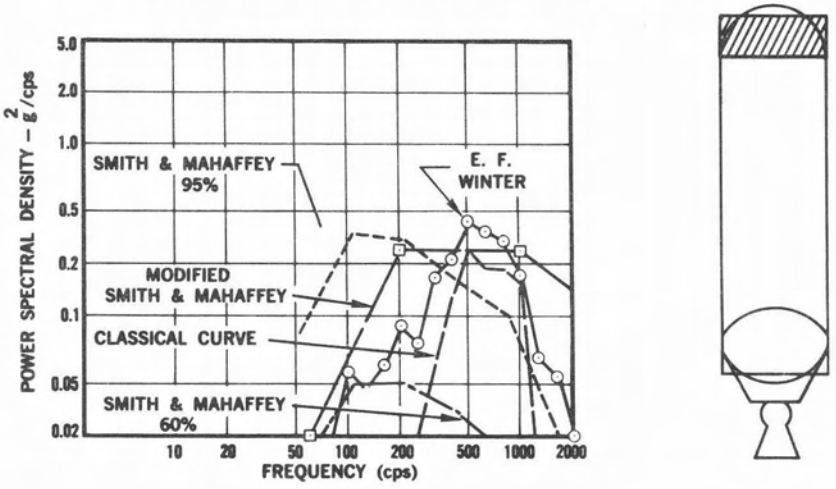

FIGURE 19

4. vibration levels determined by using the data on the classical curve of Figure 7
5. vibration levels determined by using the data of Figure 17

Three tables showing typical data on three of the prediction methods are given in addendum B of this paper. For additional information on predicting random vibration levels from Figure 7 and on sine-random conversions, the reader is referred to Reference 1. All of the curves labeled "Smith and Mahaffey" and "E. F. Winter" were determined by first finding sinusoidal vibration levels and then converting to random vibration levels by using the following equation from Reference 1:

$$G = \frac{0.174\ (Ap)^2}{f} \qquad (3)$$

where G = mean squared acceleration density or power spectral density in g^2/cps, A_p is the peak applied sinusoidal vibration, and f is the frequency of resonance.

A reasonable correlation is noticed on Figures 18 and 19. In Figure 18, the classical curve and the E. F. Winter curve display an excellent agreement. Also, the Smith and Mahaffey 95% curve and the Modified Smith and Mahaffey curve are in good agreement. The main difference is in the frequency range; this difference is a natural result of the two different techniques. The predicted random vibration levels of the S-IVB forward skirt (Figure 19) are less than the predicted vibration levels on the aft skirt. In Figure 19, all of the curves, except the Smith and Mahaffey 60% curve, compare very well. The predictions in Figures 18 and 19 provide useful vibration levels which establish a vibration gradient for the S-IVB Stage, and which are currently being used to determine S-IVB vibration test levels.

CONCLUSION

This paper has presented a brief review of the acoustic and vibration environments of the S-IV and S-IVB Stages of the Saturn Vehicle. Only a fragment of the available data was covered in this interim paper. Predictions and measurements of the acoustic and vibration environments were given. Predicted acoustic time histories for the early phases of the S-IV and S-IVB missions were presented. These acoustic predictions were compared with Saturn I flight data. Predictions of acoutic spectra for six S-IV engines (RL-10), without diffuser attenuation, were given. This presentation

included a summary of acoustic data from J-2 engine firings.

Environmental vibration levels for both the S-IV and S-IVB Stages were determined by using different methods of acoustic/vibration correlativity. Comparisons were made of the results obtained by the different correlation techniques. These methods were used to determine both sine and random vibration environments. Vibration data measured during the S-IV-5 acceptance firing were presented and discussed.

Much work remains to be done in the definition of the S-IV and S-IVB acoustical and vibrational environments. More vibration measurements will be acquired during static firings and flights of both the S-IV and S-IVB Stages. In addition, microphone measurements will be obtained. A continuous and necessary effort is underway to adequately define the acoustical and vibrational environments of the S-IV and S-IVB Stages.

ACKNOWLEDGEMENT

The writer is greatly indebted to K. E. Elliott, J. W. Lew, P. M. Lewis, J. C. McClymonds, T. D. Schoessow, P. F. Spas, and E. F. Winter of the Douglas Missile and Space Systems Division for their contributions to this paper.

REFERENCES

1. R. W. Mustain, "Prediction of Random Environments", 1963 SAE National Aeronautic and Space Engineering and Manufacturing Meeting, September 23-27 at the Ambassador, Los Angeles.
2. R. W. Mustain, "On the Prediction of Dynamic Environments", Bulletin No. 28 Shock, Vibration, and Associated Environments Part IV, Office of the Secretary of Defense, August 1960.
3. WADC Technical Report, 57-354, "Noise Radiation from Fourteen Types of Rockets in the 1000 to 130,000 Pounds Thrust Range", December 1957.
4. Northrop Report, NOR-60-26, "Structural Vibration in Space Vehicles", Phase I Report, "Investigation of Structural Vibration Sources and Characteristics".
5. WADC Technical Report 58-343, "Methods of Space Vehicle Noise Prediction", September 1960.
6. P. A. Franken and F. M. Wiener, "Estimation of Noise Levels at the Surface of a Rocket-Powered Vehicle", Bolt Beranek and Newman Inc., Los Angeles, California and Cambridge, Massachusetts.
7. P. T. Mahaffey and K. W. Smith, "A Method for Predicting Environmental Vibration Levels in Jet-Powered Vehicles", Bulletin No. 28 Shock, Vibration, and Associated Environments Part IV, Office of the Secretary of Defense, August 1960.
8. Personal communication E. F. Winter, Douglas Missile and Space Systems Division, to R. W. Mustain
9. J. C. McClymonds and J. W. Lew, "Proposed Deviation from MSFC Vibration Specification IN-P&VE-S-62-7", Douglas Missile & Space Systems Division, 4 September 1963.
10. H. Himelblau and A. G. Piersol, "Summary of Nortronics Modification of Mahaffey Smith Procedure", October 1963.

ADDENDUM A

Acoustic/vibration correlativity

I. Vibration levels determined by the method of Reference 7 (Smith and Mahaffey). The basic data for the curve (95% confidence, Smith and Mahaffey) in Figure 9 are given in Table I. These curves have been drawn through points which were plotted at the geometric mean frequencies (GMF = $\sqrt{f_1 x f_2}$) of the octave bands. Octave band widths were used in agreement with the method of Reference 7.

Table I

Octave Bands	GMF	SPL (db)	60% g's (o-peak)	95% g's (o-peak)
37.5 - 75	53	137.6	1.4	3.2
75 - 150	106	138.9	2.5	7.2
150 - 300	212	140.2	3.7	10.0
300 - 600	425	140.6	5.0	11.5
600 - 1200	850	139.0	5.2	13.3
1200 - 2400	1700	139.5	4.4	10.8

II. Vibration levels determined by using the data in Figure 6 of this paper. The calculations for the E. F. Winter curve in Figure 9 are given in Table II for the gimbal point of the S-IV Stage. This curve was determined by using the data in Figure 6 and the following basic relationship:

$$20 \log_{10} g_{rms} = SPL + TF - 20 \log_{10} W \text{ (in db re/g)}$$

where W = surface density in lb/ft^2

TF = transfer function (ordinate of Figure 6)

SPL = sound pressure level (db)

$20 \log g_{rms}$ is in db re 1 g

Table II

$20 \log_{10} W = -0.72$

1	2	3	4	5	6	7	8
Octave Band	GMF	SPL	TF	3+4	Col. 5-20 log W in db re 1g	g_{rms}	g (o-peak)
37.5 - 75	53	137.6	-148	-10.4	-9.7	.32	1.0
75 - 150	106	138.9	-143	-4.1	-3.4	.68	2.0
150 - 300	212	140.2	-138	2.2	2.9	1.40	4.2
300 - 600	425	140.6	-128	12.6	13.3	4.70	14.1
600 - 1200	850	139.0	-122	17.0	17.7	7.80	23.4
1200-2400	1700	139.5	-125	14.5	15.2	5.75	17.3

III. Vibration levels determined by using the data in the classical curve of Figure 7. The calculations for the (classical) vibration levels in Figure 9 are listed in Table III. These vibrations display a dominant peak which is characteristic of rigid primary structure. In this case, a response frequency of approximately 800 cps was assumed. Since the correlation data in Figure 7 were obtained from actual 1/3 octave acoustic and vibration measurements, they are applicable to 1/3 octave predictions. The octave-band sound pressure levels listed in Tables I and II were converted to 1/3 octave-band sound pressure levels by simply subtracting 5 db from the octave-band sound pressure levels. Table III used the relationship:

$$20 \log_{10} (g_{peak}/g_{ref}) = SPL + TF \quad \text{(in db re 0.1g)}$$

where SPL = sound pressure level in 1/3 octave bands (db)

TF = Transfer function (ordinate of Figure 7)

Table III

1	2	3	4	5	6
f 1/3 Octave Band	TF	1/3 Octave SPL (db)	Column 2 + Column 3 in db	Ratio $\frac{g\ peak}{0.1\ g}$ equivalent to db of col. 4	Col. 5x0.1 in g's (o-peak)
40	-123	132.6	9.6	3.0	.3
50	-123	132.6	9.6	3.0	.3
63	-123	132.6	9.6	3.0	.3
80	-121	133.9	12.9	4.5	.45
100	-121	133.9	12.9	4.5	.45
125	-120	133.9	13.9	5.0	.5
160	-117	135.2	18.2	8.15	.815
200	-115	135.2	20.2	10.2	1.02
250	-112	135.2	23.2	14.5	1.45
315	-108	135.6	27.6	24.0	2.40
400	-99	135.6	36.6	67.5	6.75
500	-97	135.6	38.6	85.0	8.50
630	-95	134.0	39.0	89.0	8.90
800	-94	134.0	40.0	100.0	10.0
1000	-97	135.0	37.0	71.0	7.10
1250	-100	134.5	34.5	53.0	5.30
1600	-103	134.5	31.5	38.0	3.80
2000	-104	134.5	30.5	34.0	3.40
2500	-106	134.5	28.5	26.6	2.66

ADDENDUM B

Random Vibration Predictions

I. Random vibration levels determined by the method of Reference 7 (Smith and Mahaffey) and the use of equation (3). The basic data for the Smith and Mahaffey 95% curve in Figure 18 are given in Table IV. These curves have been drawn through points which were plotted at the geometric mean frequencies (GMF = $\sqrt{f_1 x f_s}$) of the octave bands. Octave band widths were used in agreement with the method of Reference 7.

Table IV

Octave Bands	GMF	SPL (db)	95% g's (o-p)	95% g^2/cps
37.5 - 75	53	143	4.4	.07
75 - 150	106	148	13.5	.30
150 - 300	212	152	21.8	.39
300 - 600	425	152	27.0	.30
600 - 1200	850	149	29.5	.20
1200 - 2400	1700	144	15.7	.03

II. Random vibration levels determined by using the data in Figure 6 and by using equation (3). The calculations for the E. F. Winter curve in Figure 18 are given in Table V. The data in Figure 6 and the following basic relationship are used:

$$20 \log_{10} g_{rms} = SPL + TF - 20 \log_{10} W \qquad \text{(in db re 1g)}$$

Where W = surface density in lb/ft^2

TF = Transfer function (ordinate of Figure 6)

SPL = sound pressure level (db)

$W = 1\ lb/ft^2$; $20 \log W = 0$

Table V

1 f CPS	2 SPL db	3 TF db	4 Col.2 +Col.3	5 Col.4- 20 log W	6 g_{rms}	7 g(o-p)	8 g^2	9 $.174g^2$	10 g^2/cps
40	138	-150	-12	-12	0.25	0.75	0.565	.098	.0025
50	138	-148	-10	-10	0.32	0.96	0.925	.161	.0032
63	138	-147	-9	-9	0.55	1.65	2.72	.473	.0075
80	143	-146	-3	-3	0.71	2.17	5.08	.885	.0111
100	143	-144	-1	-1	1.1	3.3	10.95	1.91	.0191
125	143	-142	1	1	1.1	3.3	10.95	1.91	.0153
160	149	-139	10	10	3.17	9.5	90.4	15.75	.0985
200	149	-136	13	13	4.47	13.3	177	30.8	.154
250	149	-133	16	16	6.32	19.0	361	62.7	.251
315	149	-130	19	19	8.80	26.4	700	122	.387
400	149	-128	21	21	11.2	33.6	1134	197.5	.494
500	149	-125	24	24	15.8	47.4	2260	395	.779
630	146	-122.5	23.5	23.5	14.95	44.8	2020	351	.557
800	146	-122	24	24	15.8	47.4	2260	395	.493
1000	146	-123	23	23	14.1	42.2	1790	312	.312
1250	139	-124	15	15	5.62	16.9	286	49.7	.397
1600	139	-126	13	13	4.47	13.3	177	30.8	.193
2000	139	-126	13	13	4.47	13.3	177	30.8	.154

III. Random vibration levels determined by using the data in the classical curve of Figure 7. The calculations for the classical curve of Figure 18 are listed in Table VI. These vibrations display a dominant peak which is characteristic of rigid primary structure. In this case, a response frequency of approximately 900 cps was assumed. Since the correlation data in Figure 7 were obtained from actual 1/3 octave acoustic and vibration measurements, they are applicable to 1/3 octave predictions. Table VI uses the relationship:

$$20 \log_{10} \left(g_{peak}/g_{ref}\right) = SPL + TF \qquad \text{(in db re 0.1g)}$$

where SPL = sound pressure level in 1/3 octave bands

TF = transfer function (ordinate of Figure 7)

Table VI

1 f 1/3 octave band	2 TF	3 SPL db	4 Spectrum Level Conversion	5 20 log $\frac{g_{peak}}{0.1\ g}$	6 $\frac{g_{peak}}{0.1\ g}$	7 g peak	8 g_{rms}	9 g^2/cps
40	-123	138	-9.6	5.4	1.86	.19	.06	.004
50	-122.5	138	-10.6	4.9	1.78	.18	.06	.004
63	-122	138	-11.6	4.4	1.66	.17	.06	.004
80	-122	143	-12.6	8.4	2.63	.26	.09	.008
100	-121.5	143	-13.6	7.9	2.51	.25	.08	.006
125	-120.5	143	-14.6	7.9	2.51	.25	.08	.006
160	-118.5	147	-15.6	12.9	4.5	.45	.15	.023
200	-116	147	-16.6	14.4	5.3	.53	.18	.033
250	-112	147	-17.6	17.4	7.4	.74	.25	.063
315	-106	147	-18.6	22.4	13.3	1.33	.44	.194
400	-101	147	-19.6	26.4	20.9	2.1	.70	.49
500	-97	147	-20.6	29.4	29.5	2.95	.98	.96
630	-95	144	-21.6	27.4	23.5	2.35	.78	.61
800	-94	144	-22.6	27.4	23.5	2.35	.78	.61
1000	-94	144	-23.6	26.4	20.9	2.1	.70	.49
1250	-101	139	-24.6	13.4	4.65	.465	.15	.023
1600	-103	139	-25.6	10.4	3.31	.33	.11	.012
2000	-105	139	-26.6	7.4	2.35	.23	.08	.006